

# Non-Isothermal Kinetics of Kr Adsorption by Nanoporous $\gamma$ -Mg(BH<sub>4</sub>)<sub>2</sub> from in Situ Synchrotron Powder Diffraction

Iurii Dovgaliuk,\* Vadim Dyadkin, Mathieu Vander Donckt, Yaroslav Filinchuk,\* and Dmitry Chernyshov



Cite This: *ACS Appl. Mater. Interfaces* 2020, 12, 7710–7716



Read Online

ACCESS |



Metrics & More



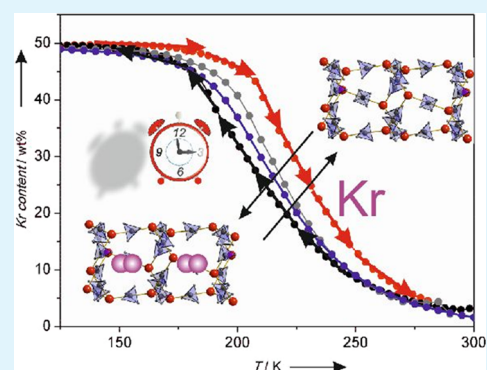
Article Recommendations



Supporting Information

**ABSTRACT:** Crystalline materials with pore dimensions comparable to the kinetic diameters of the guest molecules are attractive for their potential use in adsorption and separation applications. The nanoporous  $\gamma$ -Mg(BH<sub>4</sub>)<sub>2</sub> features one-dimensional channels matching this criterion for Kr uptake, which has been probed using synchrotron powder diffraction at various pressures and temperatures. It results in two coexisting crystalline phases with the limiting composition Mg(BH<sub>4</sub>)<sub>2</sub>·0.66Kr expecting the highest Kr content (50.7 wt % in the crystalline phase) reported for porous materials. Quasi-equilibrium isobars built from Rietveld refinements of Kr site occupancies were rationalized with a noncooperative lattice gas model, yielding the values of the thermodynamic parameters. The latter were independently confirmed from Kr fluorescence. We have also parameterized the pronounced kinetic hysteresis with a modified mean-field model adopted for the Arrhenius kinetics.

**KEYWORDS:** porous frameworks, adsorption, thermodynamics, kinetics, crystal structure



## INTRODUCTION

The efficient sorption and separation of valuable noble gases, like krypton and xenon, with extremely low concentrations in air (1.14 and 0.089 ppmv, respectively) are of great interest. Indeed, their sorption properties are similar due to close kinetic diameters (3.6 and 4.1 Å, respectively) and equally low chemical reactivities.<sup>1</sup> New methods of selective capturing carry over to the need for trapping Kr and Xe radioactive products that are generated from nuclear fission.<sup>2,3</sup> The most common way of noble gases adsorption from air or fission products requires energy-consuming cryogenic distillation.<sup>1</sup> Thus, alternative effective materials and methods are required for that purpose.

Metal–organic and other porous frameworks have been intensively studied as perspective materials for numerous applications in gas storage and separation,<sup>4,5</sup> sensing,<sup>6</sup> catalysis,<sup>7</sup> and drug delivery.<sup>8</sup> Recently, several promising metal–organic frameworks (MOFs) have been also proposed for Kr and Xe adsorption and separation.<sup>9–13</sup> The main criteria for their practical applications are based on a maximal gravimetric uptake, an isosteric heat of adsorption, and a Kr/Xe thermodynamic and kinetic selectivity. It was found that the optimal pore size of the framework channels defines the capture capability and kinetic separation of these molecules. The latter is achievable when the pore size is between one and two kinetic diameters of the molecules of interest,<sup>14–16</sup> as available in nanoporous (ultramicroporous) frameworks.  $\gamma$ -Mg(BH<sub>4</sub>)<sub>2</sub> attracted our attention as one of such perspective

nanoporous materials<sup>17</sup> due to its small pore size ( $\approx 7$  Å), matching this criterion. Its three-dimensional network of non-intersecting one-dimensional (1D) channels contains small pores separated by even narrower apertures, and thus it is a good candidate to probe thermodynamic and diffusion-controlled separation.

The characterization of volumetric and gravimetric gas uptake by  $\gamma$ -Mg(BH<sub>4</sub>)<sub>2</sub> in bulk is complicated by the inherent presence of a dense amorphous phase; its weight fraction varies from one batch to other.<sup>18,19</sup> In situ synchrotron powder diffraction enables estimation of the capacity, thermodynamics, and kinetics of Kr adsorption using temperature- and time-dependent crystallographic occupancies and fluorescence of Kr atoms exclusively from the crystalline porous  $\gamma$ -Mg(BH<sub>4</sub>)<sub>2</sub>, which is not biased by the presence of the amorphous phase. The low density of the host  $\gamma$ -Mg(BH<sub>4</sub>)<sub>2</sub> structure in combination with a high X-ray contrast of heavy Kr atoms offers a unique opportunity to study its structural response in great detail. First, good quality data allow a full structural refinement revealing a microscopic picture of adsorption from isobaric variable-temperature experiments. Second, the macroscopic properties, such as adsorption isobars and heats of

**Received:** October 24, 2019

**Accepted:** January 22, 2020

**Published:** January 22, 2020

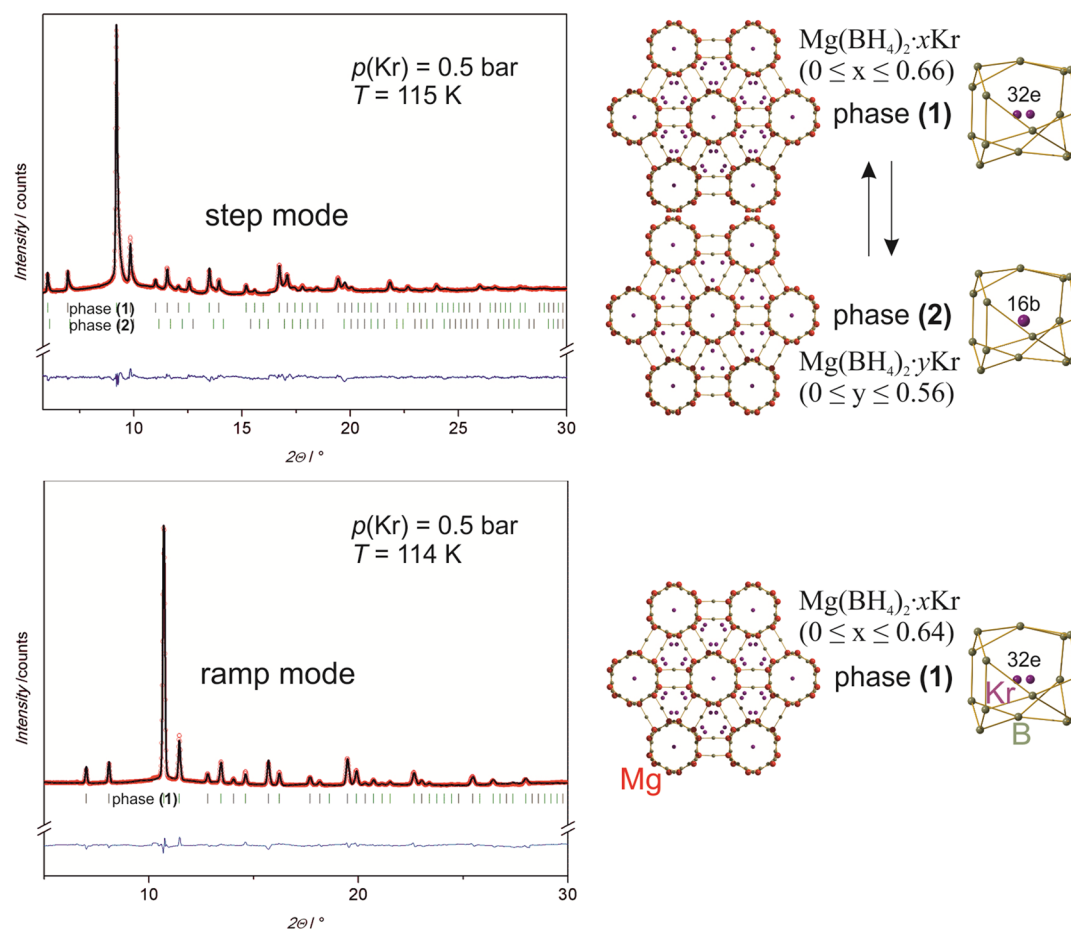


**Figure 1.** Rietveld refinement (synchrotron radiation with  $\lambda = 0.67522$  and  $0.78487$  Å for step and ramp modes, respectively) and the extracted structural models for the two phases of  $\text{Mg}(\text{BH}_4)_2 \cdot n\text{Kr}$ , at their maximal Kr uptakes. The pore fillings are shown in two projections.

adsorption, are accessed via refined Kr occupancies or by using another independent measure, the background signal. The latter, in our case, is dominated by the fluorescence from Kr, being proportional to the number of Kr atoms in the irradiated volume. The thermodynamic parameters can be obtained using the Clausius–Clapeyron relation applied to equilibrium isobars<sup>17</sup> or by using isobaric equilibrium temperature dependence using a mean-field lattice gas model.<sup>20</sup> These parameters characterize the equilibrium state of the guest molecules filling the pores. Here, we show that an in situ powder diffraction experiment with a fixed temperature ramp rate may not necessarily examine the equilibrium state. Non-equilibrium adsorption and desorption curves show ramp-dependent hysteresis that carry information on a non-isothermal kinetics. We parameterize various apparent “hysteresis” scenarios with a simple model adopted for the Arrhenius kinetics.

## RESULTS AND DISCUSSION

The data were collected at Kr pressures of 0.1 and 0.5 bar with two temperature regimes of a constant ramp rate of 6 K/min and constant step (ramp 6 K/min to a given temperature followed by waiting time of 2 min) modes; the initial aim was to detect non-isothermal kinetics effects, if any.

The powder diffraction isotherm at 298 K shows a progressive loading of Kr into the pores (Figure S1): as expected, the uptake of Kr by  $\gamma\text{-Mg}(\text{BH}_4)_2$  strongly affects the intensities of the diffraction peaks. Such a change occurs due to

a high difference between scattering (form) factors of Kr (at  $2\theta = 0$ , it is equal to the atomic number  $Z = 36$ ) and light atoms of the host structure: Mg ( $Z = 12$ ), B ( $Z = 4$ ), and H ( $Z = 1$ ). That is why Kr atoms can be easily localized close to the center of the pore by global optimization in a direct space,<sup>21</sup> while the light atoms of B and H contribute little to the total scattering picture and were fixed in our refinements. Interestingly, the refined cell parameters decrease upon Kr loading (Figure S1a). This cell contraction is due to gas adsorption and not due to the radiation damage, as the latter was reduced to the minimum by choosing the radiation dose and by doing the blank tests.

Close inspection of the data revealed diffraction peaks’ asymmetries induced by adsorption. They are hardly visible in the data collected in the ramp mode but are clearly seen for the powder patterns at high Kr loadings measured in the step mode (see Figures S2–S4). The line shape asymmetry is very similar for all the lines, ruling out  $hkl$ -dependent microstructural effects. Diffraction profiles can be very well modeled by two phases, one is similar to the empty framework while the other has broader lines and smaller cell parameters (see Figure S3c). No additional reflections or systematic absences have been observed for the broader diffraction component. We refined the two-phase model using the Rietveld method<sup>22</sup> to all the step mode data, while a single phase was fitted to the ramp mode data (see Figures S2–S4 for more details).

Rietveld refinements of the powder patterns were done sequentially along the isobars, obtaining consistent results and

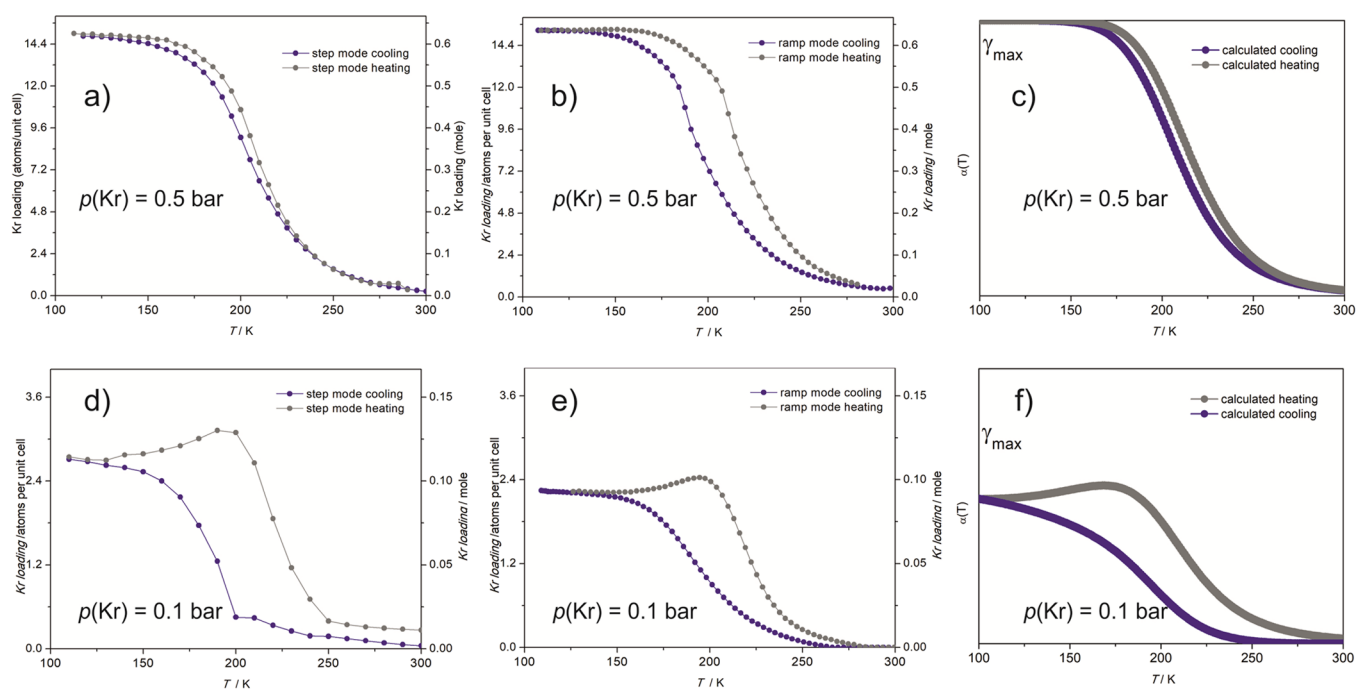


**Figure 2.** Temperature-dependent Kr adsorption isobars by  $\gamma$ -Mg(BH<sub>4</sub>)<sub>2</sub> extracted from powder diffraction data collected in the step and ramp modes (a and b for  $p(\text{Kr}) = 0.5$  bar, d and e for  $p(\text{Kr}) = 0.1$  bar) and (c and f) the modeled Kr isobars from the kinetic model (see eq 2). The contributions from phases 1 and 2 are shown in Figure S5.

good fits (see Figure 1). The phase with a larger cell parameter and sharper peaks, denoted as phase 1, is the majority phase at all temperatures. Its refined adsorption isobar shows a sigmoidal shape, with the saturation at one Kr atom per pore (16 atoms per cell or 2/3 Kr per Mg atom) (see Figure S5). Upon desorption, phase 1 releases Kr with a small hysteresis. Phase 2 is the minor phase containing smaller amounts of Kr than phase 1 (at the same conditions) (see its isobar on Figure S5). The apparent Kr-rich composition of phase 2 corresponds to  $\sim 0.84$  Kr atom per pore (14 atoms per cell or 0.56 Kr per Mg atom). Surprisingly, the cell volume for Kr-rich phase 1 is higher than that for Kr-poor phase 2, despite the cell contraction observed upon Kr loading at 298 K (Figure S1). This difference may be due to different crystal structures of phases 1 and 2. Indeed, the Rietveld refinement suggests a possible disorder of Kr around the center of the pore in phase 1 (32e Wyckoff site), while the guest takes the center of the pore in phase 2 (16b Wyckoff site) (see Figure 1 and Tables S1 and S2 with crystallographic data). In such cases, the shortest interatomic Kr–B distances will be comparable in both structures (4.13 and 4.07 Å for phase 1 and 2, respectively), while potential refinement of the Kr atomic coordinate in phase 2 is difficult due to its low fractional content (up to 30 wt %) and significant peak overlap. However, the disorder of guest atoms cannot be the sole reason for the volume difference at least at high temperatures where the Kr occupancies are nearly zero. This difference may be also related to a possible reorientation of the borohydride anions not detectable by the X-ray powder diffraction. Importantly, the mixture of the two phases of slightly different compositions is thermodynamically stable, as phase 2 appears only in the step mode, where the system is brought closer to equilibrium. Phase 2 is thus forming slower than phase 1 on loading, and it transforms back to phase 1 upon Kr unloading, as evidenced by the evolution of the weight fractions (Figure S5).

Analysis of crystal structure data in ICSD and CCDC databases<sup>23,24</sup> along with the literature on Kr adsorption<sup>9–14,25,26</sup> allows us to state that the fully loaded crystalline phase 1, Mg(BH<sub>4</sub>)<sub>2</sub>·0.66Kr, has the highest encapsulated Kr content known to date for porous materials, namely, 50.7 wt %, as evaluated from the crystallographic Kr occupancy.

A microscopic picture of Kr adsorption, described above, allows to perfectly fit a relatively simple two-phase model to all the data collected over different pressures and temperatures, both on adsorption and desorption, providing adsorption isobars, (see Figure 2a,b,d) where the Kr content is taken over the two phases (see the corresponding structure models in the Supporting Information and CCDC database: phase 1 (300 K, CCDC(1977686); 200 K, CCDC(1977685); and 114 K, CCDC(977688)) and phase 2 (300 K, CCDC(1977687); 200 K, CCDC(1977689); and 115 K, CCDC(1977690))).

The Kr content for 0.5 bar isobar shows a hysteresis for the ramp mode, which is almost suppressed for the step mode (compare Figure 2a,b). On the other hand, the isobars at 0.1 bar are highly hysteretic for both temperature regimes (see Figure 2d,e). These observations illustrate that the hysteresis is determined by the kinetics and not by cooperative effects (it is shown in ref 20 that  $\gamma$ -Mg(BH<sub>4</sub>)<sub>2</sub> is a rather rigid porous framework and cooperative effects are expected to be weak, if any). The data at 0.5 bar in the step mode can therefore be considered as the closest to the equilibrium, while the ramp mode data have to be analyzed taking the kinetics of the gas uptake into account. Indeed, the low saturation limit at 0.1 bar, well below the maximum of 16 atoms per cell, is the result of the hindered adsorption kinetics, and the upturn in the desorption isobar is very indicative for the slowed down adsorption at low temperatures.<sup>27</sup> While similar observations have been made using volumetric (picnometric) techniques,<sup>27</sup> this is the first observation of this kind using powder diffraction.

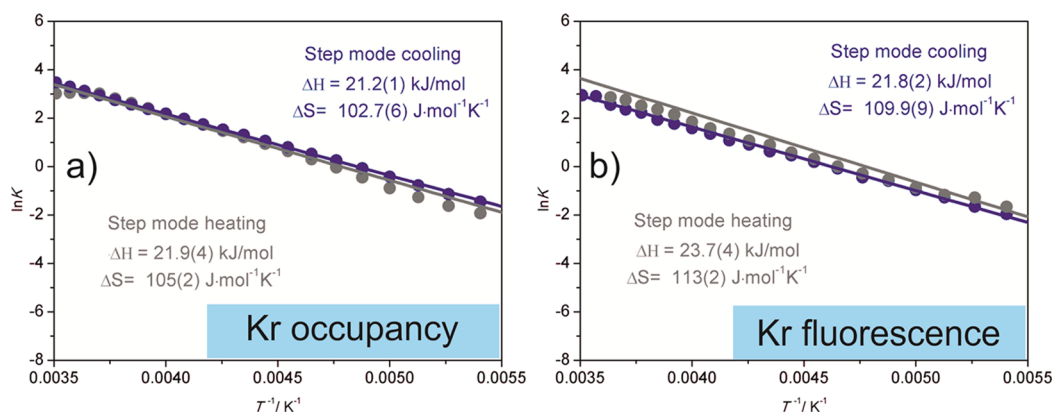


**Figure 3.** van't Hoff plots ( $p(\text{Kr}) = 0.5$  bar) obtained (a) from the refined Kr occupancies and (b) from the fluorescence signal.

The present in situ diffraction studies provide simultaneously the micro- and macroscopic information on the crystalline phase in question. It is an efficient experimental approach that allows a phenomenological study of the phase and site-specific thermodynamics of adsorption in crystalline porous solids.<sup>20</sup> The equilibrium fraction of filled guest sites for a cooperative adsorption is given in ref 20, and it is based on a mean-field lattice gas model. For  $\gamma\text{-Mg}(\text{BH}_4)_2$ , we can neglect the cooperative interactions and use a simple van't Hoff dependence for the equilibrium fraction of Kr:

$$\ln\left(\frac{\gamma}{1-\gamma}\right) = -\frac{\Delta H}{RT} + \frac{\Delta S}{R} \quad (1)$$

Here,  $\gamma$  is the fraction of the adsorbed guest molecules from the maximally achievable value at a given gas pressure. Fitting this equation to the nearly equilibrium 0.5 bar step mode isobar yields the thermodynamic parameters of adsorption:  $\Delta H$  of 21.2(1) and 21.9(4) kJ/mol for cooling and heating modes (21.6(4) kJ/mol in average) (see Figure 3a). The thermodynamic parameters extracted separately for phases 1 and 2 are comparable (Figure S7), and they suggest a slightly higher heat of Kr adsorption via the formation of phase 2. The values of the adsorption enthalpies are in good agreement with the previously reported benchmark materials for the Kr/Xe capture/separation ( $Q_{\text{st}}$ , kJ/mol): 20.1–21.4 for Noria,<sup>25</sup> 18(1) for HKUST-1,<sup>26</sup> 22 for  $\text{M}_3(\text{formate})_6$  ( $M = \text{Mn}, \text{Co}, \text{Ni}, \text{Mg}, \text{and Zn}$ ),<sup>14</sup> and 26 for SBMOF 1.<sup>12</sup>

The thermodynamics of the gas adsorption can be also parameterized to another independent observation: Kr fluorescence measured as a background signal. The latter originates from the Kr K-edge X-ray adsorption (14.3256 keV or 0.8655 Å),<sup>28</sup> achievable in our experimental conditions with a higher energy. This information is directly contained in the experimental images without the need to resort to the localization of the guest molecules, Rietveld refinements, and so on. Indeed, the temperature-dependent Kr fluorescence background behaves similar to the Kr occupancies (see Figures S8 and S9) and gives  $\Delta H = 22.8(4)$  kJ/mol (Figure 3b), very close to the values extracted from the refined Kr occupancies. This method is a powerful tool to assess the fluorescent probes and, to our knowledge, is used for the first time to quantify the thermodynamics of gas adsorption. There is a difference in the nature of the fluorescent probe: while the refined occupancies characterize the guest atoms inside the pores of the host lattice, the fluorescence accumulates both structurally coherent and noncoherent contributions from the surface, cracks, intergrain

boundaries, and other defects. Since both measures of the Kr content in the irradiated volume yield very similar results, we have evidence that the gas uptake is dominated by the Kr adsorption in the crystal pores.

Having characterized the quasi-equilibrium thermodynamics, we turn our attention to non-equilibrium isobars (Figure 2b,d,e) containing information on adsorption kinetics. We apply an approach based on a first-order reaction model.<sup>29,30</sup> Assuming the Arrhenius kinetics, being a natural choice for an Ising-like lattice model,<sup>31</sup> the temperature dependence of the apparent fraction of the occupied guest sites reads as:

$$\alpha(T) = \gamma_{\text{eq}}(T) - (\gamma_{\text{eq}}(T) - \gamma_0) \exp\left(-\frac{A}{\beta} I(T, T_0, E_a)\right) \quad (2)$$

Here,  $\gamma_0$  is the starting value of the guest occupancy (e.g., 0 on adsorption or a maximal value if we consider the desorption),  $A$  is the Arrhenius prefactor,  $\beta$  is the temperature ramp rate, and the integral function in the exponent is

$$I(T, T_0, E_a) = \int_{T_0}^T e^{-E_a/Rx} dx \quad (3)$$

where  $E_a$  is the Arrhenius activation energy and  $R$  is the gas constant.

Eq 2 models the fraction of the occupied sites as a function of temperature with finite kinetics characterized by  $A$  and  $E_a$ . The temperature is varied with the ramp rate  $\beta$ . The cooling (adsorption) branch is now below the equilibrium curve; the difference depends on the energy barrier and the cooling rate. The cooling may end up with a maximal value of the fraction  $\alpha(T_{\text{min}}) = \gamma_{\text{eq}}(T_{\text{min}}) = 1$  that would correspond to the true limiting capacity, for example, 16 Kr atoms per unit cell. In this case, the heating (desorption) starts from  $\gamma_0 = 1$ , and the entire desorption branch stays above the equilibrium curve. This is what has been observed for the step mode regime with  $p = 0.5$  bar (Figure 2b). If the cooling ends up with an incomplete adsorption,  $\alpha(T_{\text{min}}) < 1$ , this value serves as  $\gamma_0$  for the heating branch. Depending on the kinetics, the heating may give rise to a continuous desorption or to an increase in the occupancy, aiming at the equilibrium values. The latter case has been observed experimentally for  $p = 0.1$  bar (Figure 2e).

The results of the model calculations for the non-isothermal kinetics are shown in Figure 2c,f. The model with a handful of parameters obviously mimics closely the observed scenarios, indicating that the hysteresis effects indeed may be related to finite kinetics. However, quantitative estimates of the activation

energy and the elucidation of the kinetics model require a dedicated isothermal time-dependent experiment, which is the subject of our next publication. Eq 2 applied to the non-equilibrium isobars allows only for an estimate of the activation energy at 10–20 kJ/mol of Kr and the Arrhenius constant  $A$  at 0.09–0.2 min<sup>-1</sup>, thus expecting the initial adsorption rate of ~10–20% per min at room temperature. The equilibrium may therefore be reached within minutes, and a diffraction experiment aiming to map such kinetics has to be relatively fast.

Interestingly, the estimated activation barrier for Kr adsorption is of the same order as the activation energies for [BH<sub>4</sub>]<sup>-</sup> reorientations, namely, 13.3–26.6 kJ/mol in  $\beta$ - and  $\gamma$ -Mg(BH<sub>4</sub>)<sub>2</sub> polymorphs.<sup>32</sup> This hints at a possible correlation of Kr diffusion through pore apertures made of six borohydride groups with reorientational jumps of the [BH<sub>4</sub>]<sup>-</sup> tetrahedra, similar to Li-ion diffusion in *ht*-LiBH<sub>4</sub> and some other metal borohydrides.<sup>33–38</sup> This hypothesis needs verification by methods probing dynamics in the solid state.

## CONCLUSIONS

We determined a microscopic picture of Kr adsorption in  $\gamma$ -Mg(BH<sub>4</sub>)<sub>2</sub>, featuring 1D channels with apertures comparable to the kinetic radius of Kr atoms. The fully loaded phase, Mg(BH<sub>4</sub>)<sub>2</sub>·0.66Kr, has a higher crystallographic Kr content (50.7 wt %) than any other porous material. Synchrotron diffraction experiments allowed building quasi-equilibrium adsorption isobars; the latter were rationalized with the noncooperative lattice gas model, yielding the values of the thermodynamic parameters for Kr adsorption. The latter can be independently determined from a Kr fluorescence signal. This information is directly contained in the experimental images without the need to resort to the localization of the guest molecules.

The fast-ramp diffraction data, especially taken at a lower pressure, uncovers the hysteresis of kinetic origin. The model of the first-order Arrhenius kinetics with two parameters mimics closely the observed scenarios, allowing estimation of the activation energy. Observed adsorption scenarios, in particular kinetic effects, make  $\gamma$ -Mg(BH<sub>4</sub>)<sub>2</sub> an interesting candidate for separation of the Kr/Xe mixtures via selective adsorption.

Many details of the adsorption process in crystalline materials and its thermodynamic and kinetic characteristics are only possible to observe with in situ diffraction measurements like those presented in this work. Further investigations focused on the isothermal kinetic experiments with pure gases and their mixtures are the necessary next steps to determine the kinetic mechanisms and potential selectivity. Since diffraction probes the gas adsorption by the structural response of the porous crystalline phase only, it is expected to give an upper limit of the uptake. It would be also interesting to make a systematic comparison between microscopic structural and macroscopic bulk probes from gravimetric and volumetric methods; however, this task is beyond the scope of the present letter.

## EXPERIMENTAL METHODS

Detailed description of the experimental setup and structure refinement is given in the Supporting Information.  $\gamma$ -Mg(BH<sub>4</sub>)<sub>2</sub> was prepared according to ref 17. The samples of  $\gamma$ -Mg(BH<sub>4</sub>)<sub>2</sub> contain significant amounts of the amorphous Mg(BH<sub>4</sub>)<sub>2</sub> phase, different from one sample to another. Therefore, the BET surface areas cannot

be compared to data extracted from diffraction as the latter method is selective to the crystalline phase. The thermogravimetric analysis–differential scanning calorimetry data reported in ref 19 are reproducible on all our samples. The grinded powder was loaded into 0.5 mm glass capillaries in the argon-filled glovebox. A capillary filled with  $\gamma$ -Mg(BH<sub>4</sub>)<sub>2</sub> was transported into a closed Ar-filled flask prior to the diffraction measurements. The capillaries were connected to a gas-loading manifold with much larger volume, equipped with an electronic manometer (working range of 0–100 bar with 0.01% full-scale accuracy). The sample was activated at 350 K under a dynamic vacuum (turbomolecular pump) right before Kr loading. Kr pressure was set to 0.1 and 0.5 bar for variable-temperature experiments. The 298 K isotherm was measured between 0.050 and 5.600 bar with 60–120 min waiting time for each data point. The temperature was controlled using an Oxford Cryostream 700+. The temperature is varied from 300 to 115 K upon cooling followed by heating in the ramp mode (at 6 K/min rate) and in the step mode (waiting for 2 min at each temperature point).

The in situ synchrotron powder diffraction data were collected at a BM01 (SNBL/ESRF in Grenoble, France) using a PILATUS@SNBL diffractometer.<sup>39</sup> The monochromatic beam ( $\lambda = 0.78290$  Å for 298 K isotherm measurement;  $\lambda = 0.78487$  and  $0.69425$  Å for 0.5 and 0.1 bar isobars, respectively) was calibrated using LaB<sub>6</sub> powder with PyFAI.<sup>40</sup> The obtained calibrations were used in Bubble<sup>39</sup> for azimuthal integration of the two-dimensional images. The positions of Kr atoms were localized using FOX,<sup>21</sup> and the resulting structures were refined in a sequential mode by the Rietveld method in Fullprof.<sup>22</sup>

## ASSOCIATED CONTENT

### Supporting Information

The Supporting Information is available free of charge at <https://pubs.acs.org/doi/10.1021/acsami.9b19239>.

- Crystallographic data of phase1 114K ramp mode (CIF)
- Crystallographic data of phase1 200K step mode (CIF)
- Crystallographic data of phase1 300K step mode (CIF)
- Crystallographic data of phase2 115K step mode (CIF)
- Crystallographic data of phase2 200K step mode (CIF)
- Crystallographic data of phase2 300K step mode (CIF)
- Powder diffraction isotherms and all the refinements and calculations (PDF)

## AUTHOR INFORMATION

### Corresponding Authors

**Iurii Dovgaliuk** – Swiss-Norwegian Beamlines at the European Synchrotron Radiation Facility, Grenoble 38000, France; Institut des Matériaux Poreux de Paris, UMR 8004 CNRS, Ecole Normale Supérieure, Ecole Supérieure de Physique et de Chimie Industrielles de Paris, PSL Université, Paris 75005, France; [orcid.org/0000-0003-1997-4748](https://orcid.org/0000-0003-1997-4748); Email: [iurii.dovgaliuk@mail.chimie.ens.fr](mailto:iurii.dovgaliuk@mail.chimie.ens.fr)

**Yaroslav Filinchuk** – Institute of Condensed Matter and Nanosciences, Université Catholique de Louvain, B-1348 Louvain-la-Neuve, Belgium; [orcid.org/0000-0002-6146-3696](https://orcid.org/0000-0002-6146-3696); Email: [yaroslav.filinchuk@uclouvain.be](mailto:yaroslav.filinchuk@uclouvain.be)

### Authors

**Vadim Dyadkin** – Swiss-Norwegian Beamlines at the European Synchrotron Radiation Facility, Grenoble 38000, France

**Mathieu Vander Donckt** – Institute of Condensed Matter and Nanosciences, Université Catholique de Louvain, B-1348 Louvain-la-Neuve, Belgium

**Dmitry Chernyshov** – Swiss-Norwegian Beamlines at the European Synchrotron Radiation Facility, Grenoble 38000, France

Complete contact information is available at:  
<https://pubs.acs.org/10.1021/acsami.9b19239>

## Notes

The authors declare no competing financial interest.

## ACKNOWLEDGMENTS

This work was supported by FNRS (PDR T.0169.13, EQP U.N038.13, and CdR J.0164.17). We thank the ESRF for beam time allocation.

## REFERENCES

- (1) Kerry, F. G. *Industrial Gas Handbook: Gas Separation and Purification*; CRC Press: 2007.
- (2) Chen, L.; Reiss, P. S.; Chong, S. Y.; Holden, D.; Jelfs, K. E.; Hasell, T.; Little, M. A.; Kewley, A.; Briggs, M. E.; Stephenson, A.; Thomas, K. M.; Armstrong, J. A.; Bell, J.; Busto, J.; Noel, R.; Liu, J.; Strachan, D. M.; Thallapally, P. K.; Cooper, A. I. Separation of Rare Gases and Chiral Molecules by Selective Binding in Porous Organic Cages. *Nat. Mater.* **2014**, *13*, 954–960.
- (3) Liu, J.; Thallapally, P. K.; Strachan, D. Metal-Organic Frameworks for Removal of Xe and Kr from Nuclear Fuel Reprocessing Plants. *Langmuir* **2012**, *28*, 11584–11589.
- (4) Furukawa, H.; Cordova, K. E.; O’Keeffe, M.; Yaghi, O. M. The Chemistry and Applications of Metal-Organic Frameworks. *Science* **2013**, *341*, 1230444.
- (5) Adil, K.; Belmabkhout, Y.; Pillai, R. S.; Cadiau, A.; Bhatt, P. M.; Assen, A. H.; Maurin, G.; Eddaoudi, M. Gas/Vapour Separation Using Ultra-Microporous Metal-Organic Frameworks: Insights into the Structure/Separation Relationship. *Chem. Soc. Rev.* **2017**, *46*, 3402–3430.
- (6) Kreno, L. E.; Leong, K.; Farha, O. K.; Allendorf, M.; van Duyne, R. P.; Hupp, J. T. Metal-Organic Framework Materials as Chemical Sensors. *Chem. Rev.* **2012**, *112*, 1105–1125.
- (7) Doonan, C. J.; Sumbly, C. J. Metal-Organic Framework Catalysis. *CrystEngComm* **2017**, *19*, 4044–4048.
- (8) Horcajada, P.; Gref, R.; Baati, T.; Allan, P. K.; Maurin, G.; Couvreur, P.; Férey, G.; Morris, R. E.; Serre, C. Metal Organic Frameworks in Biomedicine. *Chem. Rev.* **2012**, 1232–1268.
- (9) Banerjee, D.; Simon, C. M.; Elsaidi, S. K.; Haranczyk, M.; Thallapally, P. K. Xenon Gas Separation and Storage Using Metal-Organic Frameworks. *Chem* **2018**, *4*, 466–494.
- (10) Wang, H.; Yao, K.; Zhang, Z.; Jagiello, J.; Gong, Q.; Han, Y.; Li, J. The First Example of Commensurate Adsorption of Atomic Gas in a MOF and Effective Separation of Xenon from Other Noble Gases. *Chem. Sci.* **2014**, *5*, 620–624.
- (11) Chen, X.; Plonka, A. M.; Banerjee, D.; Krishna, R.; Schaeff, H. T.; Ghose, S.; Thallapally, P. K.; Parise, J. B. Direct Observation of Xe and Kr Adsorption in a Xe-Selective Microporous Metal-Organic Framework. *J. Am. Chem. Soc.* **2015**, *137*, 7007–7010.
- (12) Banerjee, D.; Simon, C. M.; Plonka, A. M.; Motkuri, R. K.; Liu, J.; Chen, X.; Smit, B.; Parise, J. B.; Haranczyk, M.; Thallapally, P. K. Metal-Organic Framework with Optimally Selective Xenon Adsorption and Separation. *Nat. Commun* **2016**, *7*, ncomms11831.
- (13) Mohamed, M. H.; Elsaidi, S. K.; Pham, T.; Forrest, K. A.; Schaeff, H. T.; Hogan, A.; Wojtas, L.; Xu, W.; Space, B.; Zaworotko, M. J.; Thallapally, P. K. Hybrid Ultra-Microporous Materials for Selective Xenon Adsorption and Separation. *Angew. Chem., Int. Ed.* **2016**, *55*, 8285–8289.
- (14) Perry, J. J., IV; Teich-McGoldrick, S. L.; Meek, S. T.; Greathouse, J. A.; Haranczyk, M.; Allendorf, M. D. Noble Gas Adsorption in Metal-Organic Frameworks Containing Open Metal Sites. *J. Phys. Chem. C* **2014**, *118*, 11685–11698.
- (15) Sikora, B. J.; Wilmer, C. E.; Greenfield, M. L.; Snurr, R. Q. Thermodynamic analysis of Xe/Kr selectivity in over 137 000 hypothetical metal-organic frameworks. *Chem. Sci.* **2012**, *3*, 2217–2223.
- (16) Witman, M.; Ling, S.; Jawahery, S.; Boyd, P. G.; Haranczyk, M.; Slater, B.; Smit, B. The Influence of Intrinsic Framework Flexibility on Adsorption in Nanoporous Materials. *J. Am. Chem. Soc.* **2017**, *139*, 5547–5557.
- (17) Filinchuk, Y.; Richter, B.; Jensen, T. R.; Dmitriev, V.; Chernyshov, D.; Hagemann, H. Porous and Dense Magnesium Borohydride Frameworks: Synthesis, Stability, and Reversible Absorption of Guest Species. *Angew. Chem., Int. Ed.* **2011**, *50*, 11162–11166.
- (18) Stadie, N. P.; Callini, E.; Mauron, P.; Borgschulte, A.; Züttel, A. Supercritical Nitrogen Processing for the Purification of Reactive Porous Materials. *J. Visualized Exp.* **2015**, *99*, No. e52817.
- (19) Ban, V.; Soloninin, A. V.; Skripov, A. V.; Hadermann, J.; Abakumov, A.; Filinchuk, Y. Pressure-Collapsed Amorphous Mg-(BH<sub>4</sub>)<sub>2</sub>: An Ultradense Complex Hydride Showing a Reversible Transition to the Porous Framework. *J. Phys. Chem. C* **2014**, *118*, 23402–23408.
- (20) Dovgaliuk, I.; Nouar, F.; Serre, C.; Filinchuk, Y.; Chernyshov, D. Cooperative Adsorption by Porous Frameworks: Diffraction Experiment and Phenomenological Theory. *Chem. - Eur. J.* **2017**, *23*, 17714–17720.
- (21) Favre-Nicolin, V.; Černý, R. FOX, “Free Objects for Crystallography”: A Modular Approach to Ab Initio Structure Determination from Powder Diffraction. *J. Appl. Crystallogr.* **2002**, *35*, 734–743.
- (22) Rodríguez-Carvajal, J. Recent Advances in Magnetic Structure Determination by Neutron Powder Diffraction. *Phys. B* **1993**, *192*, 55–69.
- (23) Belkly, A.; Helderma, M.; Karen, V. L.; Ulkch, P. New Developments in the Inorganic Crystal Structure Database (ICSD): Accessibility in Support of Materials Research and Design. *Acta Cryst.* **2002**, *58*, 364–369.
- (24) Groom, C. R.; Bruno, I. J.; Lightfoot, M. P.; Ward, S. C. The Cambridge Structural Database. *Acta Cryst.* **2016**, *72*, 171–179.
- (25) Patil, R. S.; Banerjee, D.; Simon, C. M.; Atwood, J. L.; Thallapally, P. K. Noria: A Highly Xe-Selective Nanoporous Organic Solid. *Chem. - Eur. J.* **2016**, *22*, 12618–12623.
- (26) Hulvey, Z.; Lawler, K. V.; Qiao, Z.; Zhou, J.; Fairen-Jimenez, D.; Snurr, R. Q.; Ushakov, S. V.; Navrotsky, A.; Brown, C. M.; Forster, P. M. Noble Gas Adsorption in Copper Trimesate, HKUST-1: An Experimental and Computational Study. *J. Phys. Chem. C* **2013**, *117*, 20116–20126.
- (27) Ravikovitch, P. I.; Neimark, A. V. Diffusion-Controlled Hysteresis. *Adsorption* **2005**, *11*, 265–270.
- (28) Bearden, J. A.; Burr, A. F. Reevaluation of X-Ray Atomic Energy Levels. *Rev. Mod. Phys.* **1967**, *39*, 125–142.
- (29) Vyazovkin, S.; Wight, C. A. Isothermal and Non-Isothermal Kinetics of Thermally Stimulated Reactions of Solids. *Int. Rev. Phys. Chem.* **1998**, *17*, 407–433.
- (30) Khawam, A.; Flanagan, D. R. Solid-State Kinetic Models: Basics and Mathematical Fundamentals. *J. Phys. Chem. B* **2006**, *110*, 17315–17328.
- (31) Klinduhov, N.; Chernyshov, D.; Boukheddaden, K. Choice of Dynamics for Spin-Crossover Systems. *Phys. Rev. B* **2010**, *81*, No. 094408.
- (32) Soloninin, A. V.; Babanova, O. A.; Skripov, A. V.; Hagemann, H.; Richter, B.; Jensen, T. R.; Filinchuk, Y. NMR Study of Reorientational Motion in Alkaline-Earth Borohydrides:  $\beta$  and  $\gamma$  Phases of Mg(BH<sub>4</sub>)<sub>2</sub> and  $\alpha$  and  $\beta$  Phases of Ca(BH<sub>4</sub>)<sub>2</sub>. *J. Phys. Chem. C* **2012**, *116*, 4913–4920.
- (33) Skripov, A. V.; Soloninin, A. V.; Rude, L. H.; Jensen, T. R.; Filinchuk, Y. Nuclear Magnetic Resonance Studies of Reorientational Motion and Li Diffusion in LiBH<sub>4</sub>-LiI Solid Solutions. *J. Phys. Chem. C* **2012**, *116*, 26177–26184.
- (34) Skripov, A. V.; Soloninin, A. V.; Ley, M. B.; Jensen, T. R.; Filinchuk, Y. Nuclear Magnetic Resonance Studies of BH<sub>4</sub> Reorientations and Li Diffusion in LiLa(BH<sub>4</sub>)<sub>3</sub>Cl. *J. Phys. Chem. C* **2013**, *117*, 14965–14972.

(35) Corey, R. L.; Shane, D. T.; Bowman, R. C., Jr.; Conradi, M. S. Atomic Motions in  $\text{LiBH}_4$  by NMR. *J. Phys. Chem. C* **2008**, *112*, 18706–18710.

(36) Soloninin, A. V.; Skripov, A. V.; Buzlukov, A. L.; Stepanov, A. P. Nuclear Magnetic Resonance Study of Li and H Diffusion in the High-Temperature Solid Phase of  $\text{LiBH}_4$ . *J. Solid State Chem.* **2009**, *182*, 2357–2361.

(37) Shane, D. T.; Bowman, R. C., Jr.; Conradi, M. S. Exchange of Hydrogen Atoms between  $\text{BH}_4$  in  $\text{LiBH}_4$ . *J. Phys. Chem. C* **2009**, *113*, 5039–5042.

(38) Skripov, A. V.; Soloninin, A. V.; Filinchuk, Y.; Chernyshov, D. Nuclear Magnetic Resonance Study of the Rotational Motion and the Phase Transition in  $\text{LiBH}_4$ . *J. Phys. Chem. C* **2008**, *112*, 18701–18705.

(39) Dyadkin, V.; Pattison, P.; Dmitriev, V.; Chernyshov, D. A New Multipurpose Diffractometer PILATUS@SNBL. *J. Synchrotron Radiat.* **2016**, *23*, 825–829.

(40) Ashiotis, G.; Deschildre, A.; Nawaz, Z.; Wright, J. P.; Karkoulis, D.; Picca, F. E.; Kieffer, J. The Fast Azimuthal Integration Python Library: PyFAI. *J. Appl. Crystallogr.* **2015**, *48*, 510–519.